Unveiling the Global Oceanic Influence of Atlantic Multidecadal Variability Using Pacemaker Experiments

WEIMIN JIANG,[a] CLAUDE FRANKIGNOUL,[b] GUILLAUME GASTINEAU,[b] JULIETTE MIGNOT,[b] AND FEILI LI[a]

[a] *State Key Laboratory of Marine Environmental Science and College of Ocean and Earth Sciences, Xiamen University, Xiamen, China*
[b] *UMR LOCEAN, Sorbonne Université/CNRS/IRD/MNHN, Paris, France*

(Manuscript received 11 February 2025, in final form 1 September 2025, accepted 16 September 2025)

ABSTRACT: Atlantic multidecadal variability (AMV) significantly impacts regional and global climate, as evidenced by observations and climate model simulations. Previous sensitivity experiments investigating the AMV were mostly based on climate model simulations in which the North Atlantic sea surface temperatures (NASSTs) were nudged to a fixed AMV pattern. Here, the global influence of AMV is explored using an ensemble of pacemaker experiments where NASSTs are nudged to the time-varying observational records. Ten ensemble members proved sufficient to distinguish forced signals from internal climate variability. Using high-pass-filtered data to inform how the response to the AMV is established, we confirm that the AMV primarily affects the global ocean through its tropical component. The oceanic response to a warm AMV anomaly unfolds in four phases: 1) warming of the western Pacific warm pool and development of anomalous easterlies in the western Indo-Pacific driven by diabatic heating over the tropical Atlantic within the first 6 months, 2) eastward propagation of equatorial thermocline anomalies and establishment of La Niña–like conditions in the eastern Pacific after 7–10 months, 3) persistence of La Niña conditions during 11–20 months via Bjerknes feedback and weakening of the Aleutian low through tropical teleconnections, and 4) emergence of a negative Pacific decadal oscillation pattern in the North Pacific after 21–25 months. Our findings highlight the importance of using time-varying SST observations in pacemaker experiments to capture the full complexity of interbasin connections.

KEYWORDS: Atlantic Ocean; Atmosphere-ocean interaction; ENSO; Pacific decadal oscillation; Climate variability; Multidecadal variability

1. Introduction

Over the past century, observed North Atlantic sea surface temperatures (SSTs) have exhibited substantial variability on multidecadal time scales, commonly referred to as the Atlantic multidecadal oscillation or Atlantic multidecadal variability (AMV). This phenomenon is characterized by a basin-scale SST anomaly forming a coherent horseshoe-shaped pattern across the North Atlantic, with maximum loading in the subpolar gyre region and smaller variations in the subtropical ocean. The origin of AMV continues to be debated (e.g., Zhang et al. 2019; Robson et al. 2023). The Atlantic meridional overturning circulation (AMOC) has been identified as a main driver of AMV. Zhang et al. (2019) and Buckley and Marshall (2016) provide comprehensive reviews on the linkage between the AMOC and AMV. Stochastic atmospheric forcing also contributes to generating AMV (Clement et al. 2015; Liu et al. 2023). There has been an increasing focus on the role of external forcings in contributing to AMV. Both the natural forcing (Otterå et al. 2010; Menary and Scaife 2014; Swingedouw et al. 2015) and anthropogenic forcing (Booth et al. 2012; Bellomo et al. 2018; Bellucci et al. 2017; Watanabe and Tatebe 2019; Murphy et al. 2021; Klavans et al. 2022) influence the observed AMV.

Regarding impacts, many studies based on observations and climate models have demonstrated the association between AMV and climate variability over the surrounding continental regions, including North America, Europe, and Africa. In particular, AMV's warm (positive) phase has been linked to warmer and wetter summers over western Europe, drier summers over the Mediterranean basin (Sutton and Dong 2012; Ruprich-Robert et al. 2017), warmer and drier summers over North America (Schubert et al. 2009; Kushnir et al. 2010), and enhanced monsoon precipitation over the Sahel (Zhang and Delworth 2006; Ruprich-Robert et al. 2017). Observations suggest that a positive AMV can lead to a negative North Atlantic Oscillation (NAO) and a southward shift of the storm track in winter. Still, these linkages are not systematically reproduced in model simulations (Häkkinen et al. 2011; Gastineau et al. 2013; Peings and Magnusdottir 2014; Gastineau and Frankignoul 2015; Kwon et al. 2020; Bonnet et al. 2024).

In addition to impacting the surrounding regions, the AMV has been found to exert substantial remote influences on the global scale. The most notable teleconnections driven by the AMV occur in the tropical Pacific Ocean. The abnormal thermal low structure over the warming tropical Atlantic associated with the positive AMV phase reinforces the trade winds in the tropical Pacific and the Walker circulation (Kucharski et al. 2016; Ruprich-Robert et al. 2017). The accelerated trade winds enhance the equatorial upwelling in the central and

Denotes content that is immediately available upon publication as open access.

Supplemental information related to this paper is available at the Journals Online website: https://doi.org/10.1175/JCLI-D-25-0088.s1.

Corresponding author: W. Jiang, weimin.jiang@xmu.edu.cn

DOI: 10.1175/JCLI-D-25-0088.1

eastern Pacific, resulting in a La Niña–like cooling. In addition, Li et al. (2016) proposed that the warming of the tropical Atlantic Ocean triggers the warming over the western Indo-Pacific through a Gill-like response to the subtropical SST warming and wind–evaporation–SST feedback. This western Indo-Pacific warming might further intensify the cooling in the eastern tropical Pacific by enhancing the trade winds through the Bjerknes feedback. The driving role of the tropical Atlantic warming in the central and eastern tropical Pacific cooling is consistent with observations during the 1980–2012 period that show an important tropical Atlantic warming trend accompanied by an eastern tropical Pacific cooling (England et al. 2014; Li et al. 2016; Kosaka and Xie 2013). McGregor et al. (2018) argued that model biases in the Atlantic Ocean may cause a substantially underestimated response of the Pacific wind and surface temperature, likely implying an even stronger Atlantic–Pacific relationship in reality than in climate models. Dunstone et al. (2011) and Chafik et al. (2016) highlighted the important role of the subpolar AMV in activating the tropical AMV signal and the teleconnections with the Pacific. Other studies suggested that the AMV could modulate the multidecadal shifts of El Niño–Southern Oscillation (ENSO; Levine et al. 2017) or highlighted that the AMV influence on ENSO occurs during a negative AMO phase but not a positive phase (Geng et al. 2020).

Although interbasin interactions are typically associated with tropical regions, some studies suggested teleconnections within the midlatitudes. The AMV seems to have a significant correlation with the Pacific decadal oscillation (PDO), the leading mode of natural SST variability in the North Pacific, when AMV leads PDO (d'Orgeville and Peltier 2007; Marini and Frankignoul 2014) and may provide a source of multidecadal variability to the North Pacific through atmospheric teleconnections amplified by ocean dynamics (Zhang and Delworth 2007). On the other hand, recent studies challenged these Indo-Pacific connections with the internal AMV. Using two different climate models, as well as observations, and more advanced methods to separate internal and forced variability, Frankignoul et al. (2017) found no significant low-frequency Indo-Pacific connections with internal AMV. Fenske and Clement (2022) suggested with a large ensemble of climate models that internal connections between low-frequency climate modes in the Northern Hemisphere oceanic basins are indistinguishable from random noise. Deser and Phillips (2023) further found that the internal Atlantic–Pacific link can be artificially induced by improper removal of global warming.

The wide-ranging impacts of AMV and the controversy on the Pacific–AMV teleconnection highlight the need to better understand AMV's role in the global climate. Due to the limited observational records, many studies have relied on climate models to address the circumglobal AMV influence. However, the AMV characteristics (variance or spectrum) simulated in free-running climate models often differ substantially from the observed AMV (Coburn and Pryor 2021). To circumvent this issue, one approach is to nudge the North Atlantic SSTs toward the observational temperature records in coupled general circulation models, while allowing the SSTs outside the North Atlantic to evolve freely. All other variables follow the standard equations of the climate model. The North Atlantic SSTs can be restored to either a time-invariant AMV pattern (Ruprich-Robert et al. 2017; Meehl et al. 2021) or time-evolving North Atlantic temperatures (Si et al. 2023). The former is often referred to as idealized pacemaker experiments, and the latter is often referred to as transient. Using idealized pacemaker experiments with a fixed AMV pattern derived from observations and focusing on the quasi-equilibrium model response, Ruprich-Robert et al. (2017) found in two climate models a winter La Niña–like response to the winter-to-spring positive AMV occurring through Walker circulation changes triggered by the tropical part of the AMV. Meehl et al. (2021) further confirmed weak opposite-sign SST changes in the tropical Pacific when a fixed AMV pattern is specified in the Atlantic. However, Kim et al. (2020) and O'Reilly et al. (2023) noted that the nudging applied in the tropical Atlantic when using a fixed AMV pattern leads to an unrealistic positive surface heat input into the atmosphere. This may result in overestimated precipitation changes in the tropical North Atlantic and exaggerated teleconnections with other tropical basins. The challenges in interpreting the impact of AMV using idealized pacemaker experiments call for alternative methods to explore the AMV's influences. Si et al. (2023) used transient experiments with North Atlantic SSTs nudged toward time-varying SST observations and found that the AMV impacts on midlatitude climates resemble the observations to a certain degree. They noted that the geographical positions of action centers for precipitation and surface air temperature anomalies generally match observations, although not for the sea level pressure (SLP). However, the mechanisms linking the Atlantic Ocean to other basins were not discussed in detail by Si et al. (2023).

Here, we explore the interbasin teleconnections linked to the AMV and associated mechanisms with transient pacemaker experiments using time-varying SSTs in the North Atlantic. The paper is organized as follows. Section 2 introduces the pacemaker experiments and the AMV. In section 3, the main features of the pacemaker experiments are described. Section 4 investigates the responses of the Indian and Pacific Oceans to the tropical AMV, and section 5 provides a summary and discussion.

2. Methodology

a. The pacemaker experiments

The experiments are performed with the IPSL-CM6A-LR climate model, which is the Coupled Model Intercomparison Project phase 6 (CMIP6) version of the IPSL climate model (Boucher et al. 2020). Its atmospheric component LMDZ6 has a resolution of 1.26° × 2.5° and 79 levels with a top level at 1 Pa. The ocean model NEMO uses the ORCA1 grid with 75 levels and a resolution of ~1°, refined to 1/3° in the equatorial and polar regions. The land component is ORCHIDEE in the same horizontal grid as the atmosphere model. The sea ice module LIM3.6 adopts five sea ice categories. We also use

a 32-member ensemble of historical simulations extended after 2014 using shared socioeconomic pathway (SSP) 245 forcings and covering the period 1850–2059 (Bonnet et al. 2021) and a 500-yr preindustrial control simulation from the same model.

The Atlantic pacemaker experiment follows the protocol of the component C of the Decadal Climate Prediction Project (DCPP-C; Boer et al. 2016). Among the experiments described in DCPP-C, the one used is referred to as dcppC-atl-pacemaker. The North Atlantic SSTs are restored to a target constructed as the sum of the model's climatological seasonal cycle in the 1950–2014 period and observed monthly SST anomalies that are relative to the same 1950–2014 period from ERSSTv4 (Huang et al. 2016). The anomalies are smoothed with a 12-month running mean before being used for nudging. The nudging is applied to the Atlantic between 10° and 65°N, with two additional 8° buffer zones along the meridional boundaries to prevent discontinuities between the restored and unrestored regions (see DCPP-C technical note I: https://www.wcrp-climate.org/wgsip/documents/Tech-Note-1.pdf). Outside the restoring region, the SST is free to evolve. SST nudging is applied with a moderate strength of 40 W m^{-2} K^{-1}, equivalent to a restoring time scale of about 60 days for a 50-m mixed layer depth (see DCPP-C technical note II: https://www.wcrp-climate.org/wgsip/documents/Tech-Note-2.pdf). The pacemaker ensemble simulation comprises 10 ensemble members, starting on 31 December 1919 from initial conditions taken from 10 historical simulations. The simulation is run from 1920 to 2014 using external forcing from CMIP6 historical simulations.

Additional experiments are produced by nudging SST anomalies only in the subpolar Atlantic (80°W–0°, 30°–60°N, with 5° buffer zones in the northern and southern frontiers). These simulations, referred to as *subpolar pacemaker* experiments, run from 1950 to 2021 and consist of 20 members with initial conditions from existing historical simulations. The pacemaker experiments discussed in the following denote the experiment with nudging fully applied from 10° to 65°N unless otherwise specified.

To focus solely on internal climate variability, we remove the effect of external forcing by subtracting the ensemble mean of the 32 extended historical simulations from all *pacemaker* simulations. Although this method may introduce biases in estimating internal Atlantic–Pacific connections due to slight differences in forced warming trends between pacemaker and historical simulations (Bonnet et al. 2021; see also Fig. S1 in the online supplemental material), the impact is expected to be minimal when focusing on changes that occur within a few years. The seasonal cycle is removed at each grid point before the analysis.

In each pacemaker simulation, SST anomalies are driven by both the nudging and the internal model variability. The latter is uncorrelated between realizations, and averaging over multiple ensemble members can reduce this internal variability, thus emphasizing response to the nudged SSTs and external forcings. However, when the ensemble size is small, it needs to be verified whether the internal variability is efficiently removed by ensemble averaging. This issue is investigated in section 3. We also used signal-to-noise pattern filtering from pacemaker and historical simulations (Wills et al. 2020) as an alternative to ensemble averaging, but the results were nearly identical (not shown).

b. Definition of AMV

The AMV index is defined as the 10-yr low-pass-filtered SST anomalies averaged in the North Atlantic (0°–75°W, 0°–65°N). We employ a third-order Butterworth filter with a 10-yr cutoff period for low-pass filtering. Reflective padding is used at the beginning and the end of time series to account for edge effects introduced by filtering. The associated AMV pattern is obtained by regressing 10-yr low-pass-filtered SST anomalies on the standardized AMV index. Figure 1a compares the mean AMV index of the pacemaker experiments (10°–65°N Atlantic nudged) with the corresponding one derived from observations (ERSSTv4), where the global warming signal at each grid point is estimated and removed by regression onto the area-weighted global-mean SST. Both AMV indices display similar behavior with pronounced multidecadal variability, including a peak around 1945 followed by a drop through 1950 (Fig. 1a), also evident in the global-mean SST (Fig. S1). This midcentury decline may partly reflect observational biases present in early historical datasets (Chan et al. 2024). The simulated AMV exhibits a somewhat weaker amplitude before the 1970s. The associated simulated SST pattern (Fig. 1c) also shows a smaller amplitude (~0.6°C) in the subpolar gyre compared to the observed one (0.8°C, Fig. 1b). In the tropical Atlantic, the SST magnitudes are similar, ~0.3°C, but the simulation underestimates warming on the western side. The overall AMV underestimation likely results from the relatively moderate nudging strength, which does not fully restore model SST anomalies to the observed values.

To understand the respective contributions of the extratropical and tropical parts of the AMV in pacemaker experiments, we divide the AMV domain into subpolar and tropical domains. We define thereby three AMV time series, namely, T_{full}, T_{trop}, and T_{subp} by projecting the raw monthly SST onto the AMV pattern in the full, tropical, and subpolar domains, respectively (see Fig. 1c). For example, T_{full} is defined with

$$\mathrm{T}_{\text{full}}(t) = \frac{\sum_x w_{\text{full}}(x) T_{\text{AMV}}(x) \mathrm{SST}(x, t)}{\sum_x w_{\text{full}}(x) T_{\text{AMV}}(x) T_{\text{AMV}}(x)}, \tag{1}$$

where x and t are the horizontal grid and time indices, respectively. The $T_{\text{AMV}}(x)$ denotes the AMV pattern, and $\mathrm{SST}(x, t)$ denotes the SST. The $w_{\text{full}}(x)$ is the gridpoint area over the full domain and is zero elsewhere. The subpolar AMV (T_{subp}) is identical but uses $w_{\text{subp}}(x)$ with nonzero spanning from 0° to 70°W and from 30° to 65°N, while the tropical part (T_{trop}) extends from 0° to 70°W and from 5° to 28°N. With such a projection, an index of one corresponds to a typical AMV magnitude. The simulated raw full AMV index (Fig. 1d, black) consists of low-frequency variations on the multidecadal scale and high-frequency fluctuations. The subpolar AMV index (Fig. 1d, blue) closely resembles the full one, as

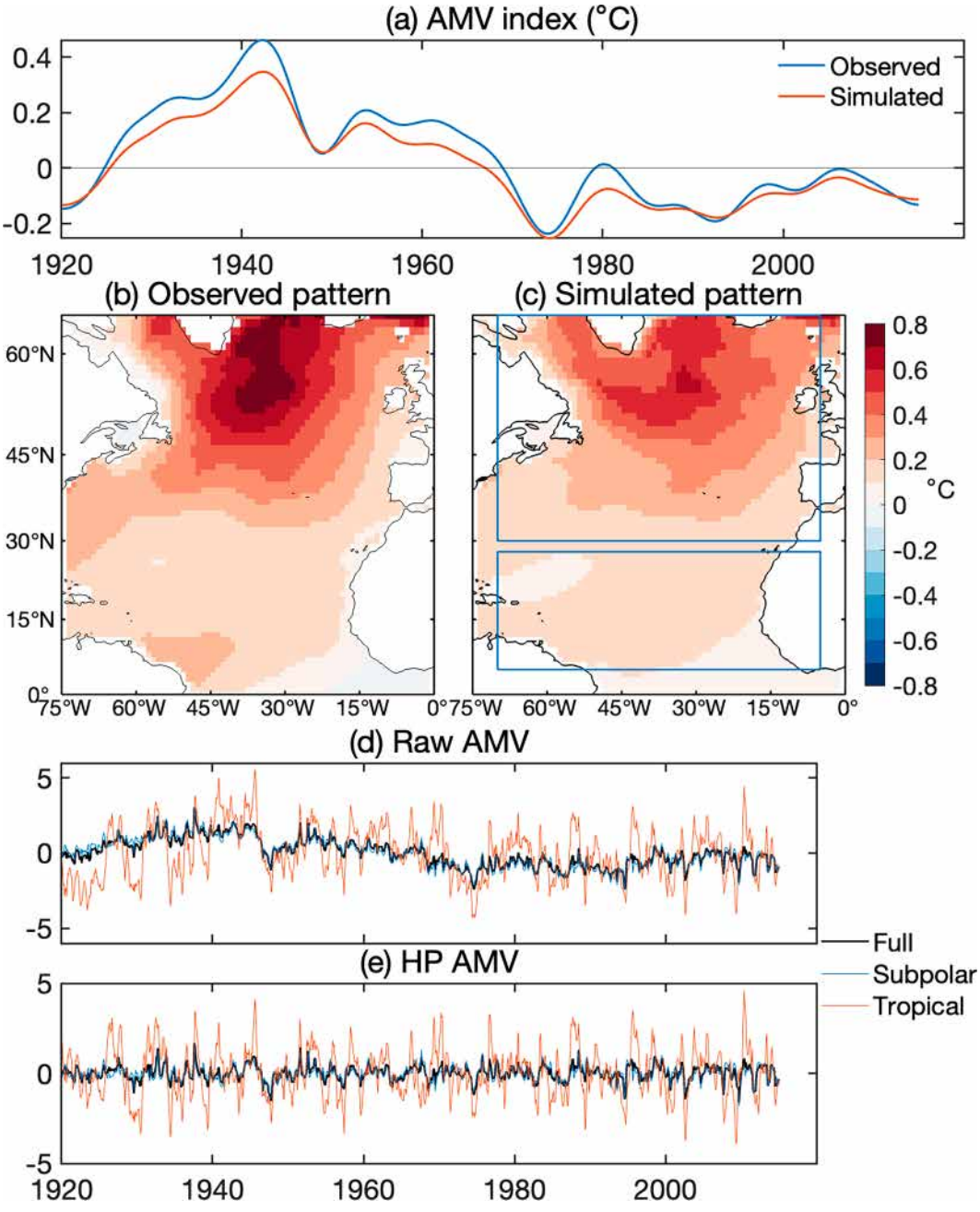

FIG. 1. (a) Observed (blue) and ensemble-mean pacemaker simulated (orange) AMV time series (°C). (b) Observed AMV pattern (°C). (c) As in (b), but for pacemaker simulations. Two blue boxes indicate the definition of the subpolar and tropical AMV regions used in this study. (d) Ensemble-mean monthly full (black), subpolar (blue), and tropical (orange) AMV indices (dimensionless) in the pacemaker simulation, defined by projecting the monthly SST anomalies onto the entire, subpolar, and tropical AMV patterns in (c), respectively. (e) As in (d), but for 10-yr high-pass-filtered AMV indices.

the low-frequency SST variance is largest in the subpolar domain. Conversely, the simulated tropical AMV (Fig. 1d, orange) fluctuates on shorter time scales than the full AMV, and its amplitude often exceeds that of the extratropical or full AMV.

To investigate how the AMV influences other basins on relatively short time scales, we apply a high-pass filter to the AMV indices (Fig. 1e) by subtracting the 10-yr low-pass fluctuations from the raw time series. The same high-pass filtering is applied to the other fields of interest.

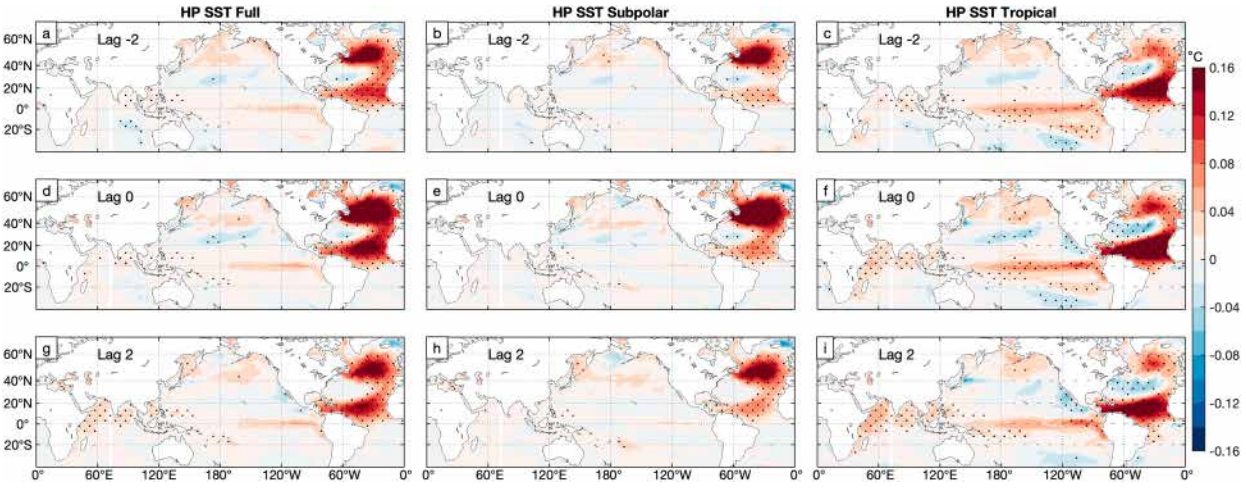

FIG. 2. Lead–lag regression of the ensemble-mean pacemaker high-pass-filtered SST anomalies (°C), onto normalized ensemble-mean high-pass-filtered (a),(d),(g) AMV T_{full}, (b),(e),(h) subpolar AMV T_{subp}, and (c),(f),(i) tropical AMV T_{trop} from pacemaker simulations. The lag is in months. AMV leads at positive lag. Lags (top) −2, (middle) 0, and (bottom) 2. Dots indicate statistical significance at the 5% level.

c. *Statistical analysis*

To investigate the response to the simulated AMV, we use lead–lag correlations and regressions, with lag measured in months. The level of significance for correlation based on ensemble-mean time series is estimated using a *t* test, thus assuming a Gaussian distribution. To account for the time autocorrelation, the effective degree of freedom for the test is determined using the method of Pyper and Peterman (1998). When averaging the correlations among individual ensemble members, we calculate the confidence interval of the mean correlation based on Gaussian distribution.

3. Evaluation of simulations

a. *Subpolar and tropical AMVs*

Assuming that the processes leading to interbasin connections can be best understood by investigating the short-term variability, we focus on 10-yr high-pass-filtered variables. As illustrated in Fig. 2, lead–lag regressions of the ensemble-mean SST anomalies onto the AMV indices in pacemaker simulations suggest limited short time-scale links between T_{subp} and SST in other basins (Figs. 2b,e,h). In the North Atlantic Ocean, regressions on T_{full} (Figs. 2a,d,g) resemble the weighted superposition of those on the subpolar (Figs. 2b,e,h) and tropical (Figs. 2c,f,i) indices. This similarity also occurs at larger lags (not shown). On short time scales, the subpolar AMV thus appears to have limited global teleconnections.

Consistently, the lead–lag correlations between the Niño-3 SST index (area-weighted SST anomalies averaged over 5°S–5°N and 150°–90°W; denoted as Niño-3) and T_{subp} are negligible, with correlations ranging between −0.12 and 0.1 (Fig. 3a, black curve). The same holds in the subpolar pacemaker experiments (Fig. 3a, red curve), confirming the lack of significant global teleconnections with the subpolar AMV at short time scales. On the other hand, T_{trop} shows significant links with the tropical Indo-Pacific (Figs. 2c,f,i). In the following, we therefore focus solely on the global links with the tropical AMV.

In the pacemaker simulations, warming in the equatorial Pacific, with maximum anomalies in the eastern Pacific, is observed in phase (lag = 0) with the tropical Atlantic SST (Fig. 2f). It is significant at the 5% level between 2 months before (Fig. 2c) and 2 months after T_{trop} (Fig. 2i). The links between the tropical AMV and the equatorial Pacific at larger lags are illustrated by the lag correlation between Niño-3 and T_{trop} (Fig. 3b, black curve). There is a small but significant positive peak around lag 0 (correlation $r = 0.18$) and a larger negative correlation ($r = -0.35$) when Niño-3 follows T_{trop} by ~14 months. In contrast, the tropical AMV exhibits the largest correlation when Niño-3 leads by 6 months in observations (blue curve, $r = 0.48$), although there is also a significant negative correlation when Niño-3 lags by ~12 months. The same analysis in the preindustrial control simulation shows similar features, but the correlation when Niño-3 leads by 6 months is smaller than when it lags (orange curve). Considering that the autocorrelation of Niño-3 reaches a minimum of −0.49 at lag 17 in the preindustrial control run and −0.46 around lag 20 in observations (not shown), the lag difference between the positive and negative peaks in Fig. 3b (17 and 19 months, respectively) closely matches the autocorrelation minima of Niño-3. This may broadly reflect the oscillatory character of Niño-3 in the control run and observations. It is nevertheless difficult to distinguish the cause and effect when the entire ocean is free to evolve. In pacemaker experiments, however, ENSO forcing of the tropical Atlantic is strongly damped by the SST nudging, which explains the different cross-correlation shape and the much smaller correlation when Niño-3 leads. Nonetheless, Fig. 3b also shows a strong negative correlation when T_{trop} leads Niño-3. This raises two questions about the pacemaker experiments: 1) Is the tropical AMV still affected by ENSO despite the nudging?

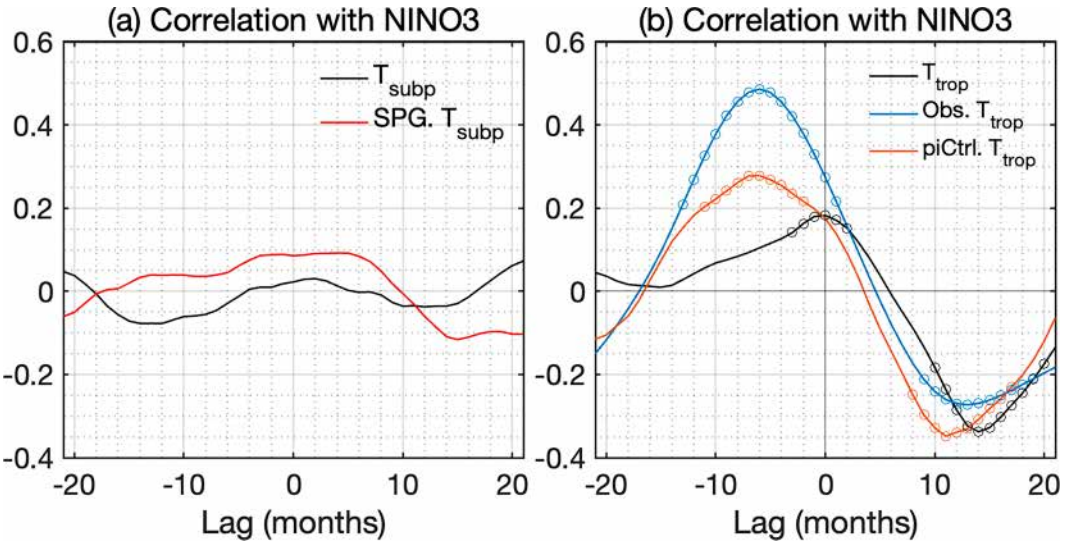

FIG. 3. (a) Lead–lag correlations between T_{subp} and Niño-3 in ensemble-mean pacemaker simulations (black) and ensemble-mean subpolar pacemaker experiments (red). No correlation is significant at the 5% level. (b) Lead–lag correlations between T_{trop} and Niño-3 in ensemble-mean pacemaker simulations (black), preindustrial control simulation (orange), and observations (blue). Circles indicate 5% significance.

2) Can one interpret the negative correlation near lag 14 as a tropical Pacific response to the tropical AMV? In other words, is the internal variability in the pacemaker experiments sufficiently damped by averaging over 10 ensemble members? To address these questions and evaluate the performance of the pacemaker experiments, we develop next a simple statistical model.

b. *Simplified SST model*

Here, the tropical AMV index for each ensemble member, its ensemble average, and the deviation of each member from the ensemble average are examined. These indices are denoted by $T_{trop}(t)$, $\overline{T_{trop}}(t)$ and $T'_{trop}(t)$, respectively. The overbar denotes the ensemble averaging, while the prime designates deviation from the ensemble mean. The same convention applies to other indices.

Based on a classical slab mixed layer ocean model (Frankignoul and Hasselmann 1977), an oceanic mixed layer of constant depth h is forced by SST nudging and a heat flux linked to the internal atmospheric variability. This model can be used in a first approximation in the tropical AMV domain (0°–70°W, 5°–28°N) because this domain largely excludes equatorial waves and the strong currents associated with the coastal upwelling in the Gulf of Guinea. The rate of change of T_{trop} is approximated by

$$\partial_t T_{trop}(t) = k[\theta_{trop}(t) - T_{trop}(t)] - \lambda T_{trop}(t) + f(t) + R(t), \tag{2}$$

where t is the time in month and λ represents the SST damping via air–sea fluxes, diffusion, and entrainment. The $\theta_{trop}(t)$ is the observed tropical AMV time series obtained by projecting the observed SST onto the observed tropical AMV pattern derived as in Eq. (1). The nudging strength, $k = \gamma/\rho C_p h$, is expressed in s^{-1}, where $\gamma = 40$ W m^{-2}, ρ is the seawater density, C_p is the specific heat capacity, and h is the mixed layer depth. The $f(t)$ represents the heat flux forcing from the atmosphere, which can arise either from local or remote variability. We use $h = 30$ m for the tropical Atlantic based on the mean mixed layer depth (de Boyer Montégut et al. 2004) and $\lambda = (6 \text{ months})^{-1}$, consistent with the e-folding scale of T_{trop} (not shown). A residual term $R(t)$ is added to Eq. (2) to account for the oversimplifications of the slab model, which neglects seasonality, horizontal advection, and entrainment processes. Using a centered finite difference to approximate the time derivative, Eq. (2) is reformulated as

$$[T_{trop}(t+1) - T_{trop}(t-1)]/2\Delta t = k\theta(t) - (\lambda + k)T_{trop}(t) + f(t) + R(t). \tag{3}$$

Hereafter, all terms of Eq. (3) are high-pass filtered to focus on the short-term response to the tropical AMV.

We now investigate possible components of $f(t)$. As suggested by Fig. 2c, the tropical Pacific and Indian Ocean warming leads the tropical AMV, indicating potential forcing roles of Pacific (Fig. 3b) and Indian Ocean SSTs. The tropical Pacific SSTs are characterized by the Niño-3 index, hereafter noted $P(t)$. Similarly, the Indian Ocean SSTs are represented by an SST index $I(t)$, defined as area-weighted SST anomalies averaged over 0°–20°N and 40°–120°E. Additionally, the NAO and other modes of internal atmospheric variability also influence the tropical AMV (e.g., Gastineau and Frankignoul 2015). To account for the atmospheric circulation's forcing on the tropical AMV, we regress the concatenated SLP in each member onto the concatenated $T_{trop}(t)$ index. The resulting mean SLP pattern (Fig. 4a)

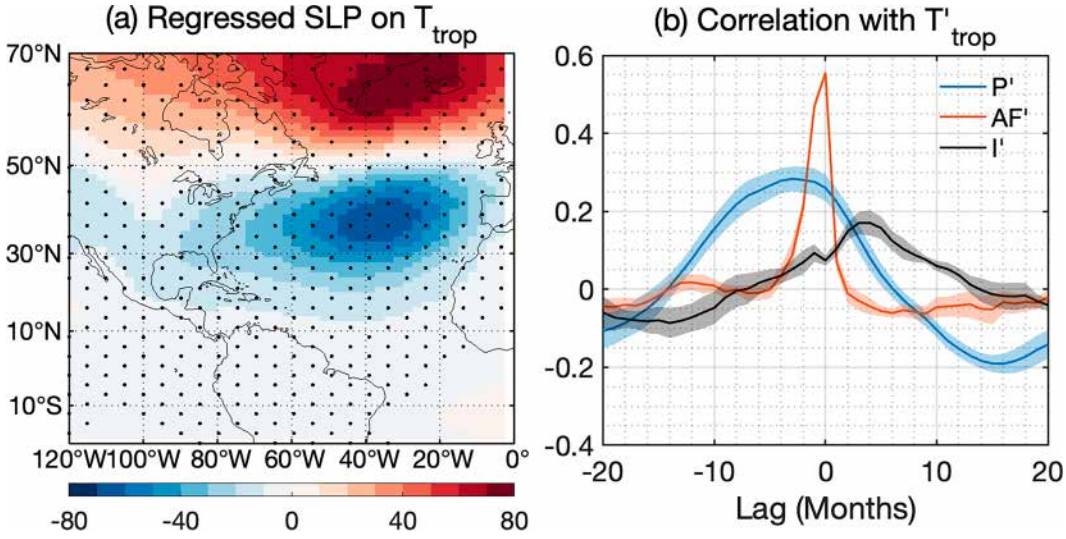

FIG. 4. (a) In phase regression of concatenated SLP in each ensemble member (Pa), on the concatenated high-pass tropical AMV, T_{trop}. (b) Lead–lag correlation between the high-pass T'_{trop} and Niño-3 index P′ (blue), atmospheric forcing AF′ (orange), and Indian SST index I′ (black). Solid lines show the averaged correlations over all ensemble members, and shadings indicate the 95% confidence interval. The T'_{trop} leads at positive lag. Both panels are based on the pacemaker experiments.

broadly resembles a negative phase of the NAO. Time series of the local atmospheric forcing, denoted AF(t), are derived by projecting the monthly SLP onto this pattern over the region 5°–35°N, 70°–10°W in each ensemble member as in Eq. (1). As we are seeking to characterize the local tropical atmospheric forcing, AF(t) is defined using a relatively narrow tropical region.

To estimate these various contributions, we analyze deviations from the ensemble average in the 10-member pacemaker simulations. This provides $T'_{\text{trop}}(t)$, $P'(t)$, $I'(t)$, and AF′(t) indices for the 10 ensemble members, which primarily represent internal variability. As shown in Fig. 4b, the averaged cross correlation between $T'_{\text{trop}}(t)$ and $P'(t)$ displays a positive peak at lag −3, indicating significant ENSO forcing on the $T'_{\text{trop}}(t)$. The atmospheric forcing AF′(t) also significantly leads $T'_{\text{trop}}(t)$ by 0–1 month, consistent with the expected time lag between stochastic atmospheric forcing and SST response when the mixed layer is shallow (Frankignoul and Hasselmann 1977). In contrast, the correlation between T'_{trop} and the Indian Ocean SST index $I'(t)$ peaks at positive lags and is small when $I'(t)$ leads. This suggests that the Indian Ocean responds to the AMV rather than forces it.

Based on these analyses, the atmospheric forcing in Eq. (2) is approximated by $f(t) = aP(t-3) + b\,\text{AF}(t)$, where a and b are two constants. For simplicity, we choose a time lag of 3 months for the P forcing, though the results below are not very sensitive to this lag. Equation (2) can now be written as

$$\text{TRD}(t+1) = k\theta(t) + aP(t-3) + b\text{AF}(t) + R_s(t), \qquad (4)$$

where TRD represents the rate of change of T_{trop} and its damping:

$$\text{TRD}(t+1) = \frac{T_{\text{trop}}(t+1) - T_{\text{trop}}(t-1)}{2\Delta t} + (\lambda + k)T_{\text{trop}}(t). \qquad (5)$$

Here, R_s is the residual R from Eq. (2), augmented by the additional forcing factors not represented by AF and P. Subtracting the ensemble mean from each member removes the nudging term since it does not vary between members, yielding

$$\text{TRD}'(t+1) = aP'(t-3) + b\text{AF}'(t) + R'_s(t). \qquad (6)$$

Here, R'_s is uncorrelated with both P' and AF′ across ensemble members (not shown), except for a very weak correlation (∼−0.08) between $R'_s(t)$ and $P'(t-3)$ in a single member, which is unlikely to influence the regression results. Therefore, the coefficients a and b are estimated using bivariate regression in each member. Their averaged values across the 10 members are 0.304°C^{-1} month^{-1} (ranging from 0.234° to 0.342°C^{-1} month^{-1}) and 0.169 month^{-1} (ranging from 0.164 to 0.18 month^{-1}), respectively, different from zero at 5% significance level. The averaged variance of TRD′($t+1$), $aP'(t-3)$, bAF′(t), and $R'(t)$ is, in units of month^{-2}, 1.18, 0.07, 0.5, and 0.613, respectively. Local atmospheric forcing dominates while ENSO plays a minor role. The residual accounts for about half of the variance of the right-hand side of Eq. (6), as R'_s represents unresolved processes such as seasonal effects, horizontal advection, vertical diffusion, entrainment, and potential additional forcings not captured by AF′(t) and $P'(t-3)$. Given its simplicity, the SST model is adequate to assess whether internal atmospheric variability in the pacemaker experiments is sufficiently reduced by

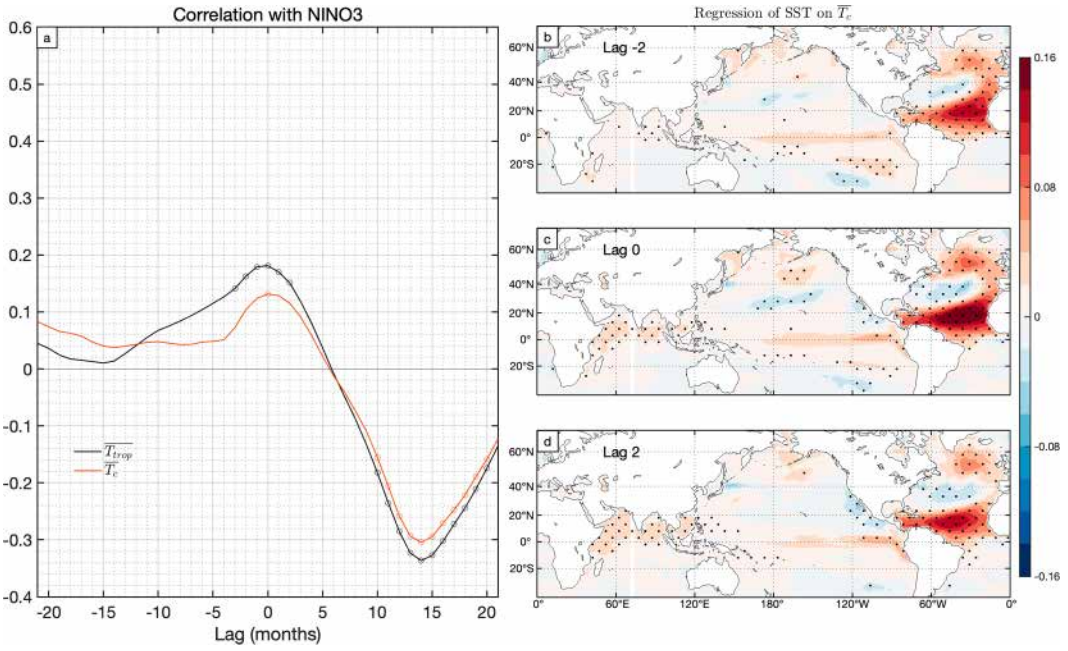

FIG. 5. (a) Lead–lag correlations between high-pass-filtered Niño-3, $\overline{P}$, and actual ($\overline{T_{\text{trop}}}$; black) and reconstructed ($\overline{T_c}$; orange) tropical AMV index in the ensemble-mean pacemaker simulation. (b)–(d) Regression of $\overline{\text{SST}}$ on $\overline{T_c}$ at lag −2, 0, and 2, as indicated. Lag is in months. AMV leads at positive lag. Circles in (a) or dots in (b)–(d) indicate statistical significance at the 5% level.

ensemble averaging, thereby enabling a robust attribution of AMV-induced impacts on other basins.

When Eq. (4) is applied to the ensemble means, however, the variance of $\overline{\text{TRD}}(t+1)$, $k\theta(t)$, $a\overline{P}(t-3)$, and $b\overline{\text{AF}}(t)$ is 2.16, 1.07, 0.01, and 0.06 month^{-2}, respectively. The nudging largely dominates the AMV evolution, with ENSO and SLP forcing explaining only 3% of the variance of $\overline{\text{TRD}}(t+1)$, reflecting that natural forcing is uncorrelated between members. Nonetheless, as discussed in section 3a, the significant correlation between ensemble-mean Niño-3 and tropical AMV (Fig. 3b, black curves) still implies that internal variability is not entirely eliminated by the ensemble average of 10 members, although it does not play an important role in forcing the tropical AMV.

This can be further validated by constructing a new tropical AMV index $T_c(t)$, obtained by integrating Eq. (4) without our estimates of the two internal forcing terms $aP(t-3)$ and $b\text{AF}(t)$. For numerical stability, we use a forward form of the time derivative. Taking ensemble mean leads to the reconstructed $\overline{T_c}(t)$ which estimates $\overline{T_{\text{trop}}}$ with a strongly reduced imprint of internal variability. Figure 5a confirms that $\overline{T_c}(t)$ and $\overline{T_{\text{trop}}}$ are very close, but the positive correlation peak between Niño-3 and the tropical AMV at short lags is reduced by using $\overline{T_c}$, mostly losing statistical significance (orange line). Similar results are found in the regression maps of ensemble-mean SST on $\overline{T_c}$ (Figs. 5b,c): At lag −2, the tropical Pacific warming is strongly reduced (cf. with Fig. 2c). This suggests that the significant tropical Pacific regressions in Fig. 2c mainly reflect the forcing of the tropical AMV by internal variability rather than a response to the AMV. In addition, the tropical Indian Ocean warming is barely affected and keeps growing from lag −2 to lag 2 (Figs. 2f–i and 5c,d) or 3 (not shown) and then slowly decreasing at larger lags, which confirms that the Indian Ocean warming is a response to tropical atmospheric circulation changes driven by the tropical AMV. On the other hand, the negative correlation when Niño-3 lags $\overline{T_{\text{trop}}}$ by about 14 months appears largely unaffected by internal variability (cf. black and orange lines in Fig. 5a), suggesting a robust Pacific response to the tropical AMV. Given that both the short-lag Indian Ocean warming (lags 0–2 months) and the delayed Pacific cooling (~14 months) are robust features, the following section investigates the mechanisms linking these responses—particularly how the early Indian warming may initiate the subsequent development of La Niña–like conditions in the tropical Pacific. Furthermore, as the ensemble mean effectively suppresses internal variability (Fig. 5a), the mechanisms can be safely diagnosed using the ensemble mean of the pacemaker simulation.

4. Response to AMV

We now explore the transient mechanisms through which tropical AMV influences the Indo-Pacific climate. High-pass-filtered ensemble averages from the pacemaker simulations are used to focus on the short-term response to the tropical AMV. Regressions of key atmospheric and oceanic fields onto the tropical AMV index are presented to reveal the sequence of responses across basins.

We first focus on responses within the first 2 months, presented in Figs. 2 and 6. In phase with $\overline{T_{\text{trop}}}$, the warmer

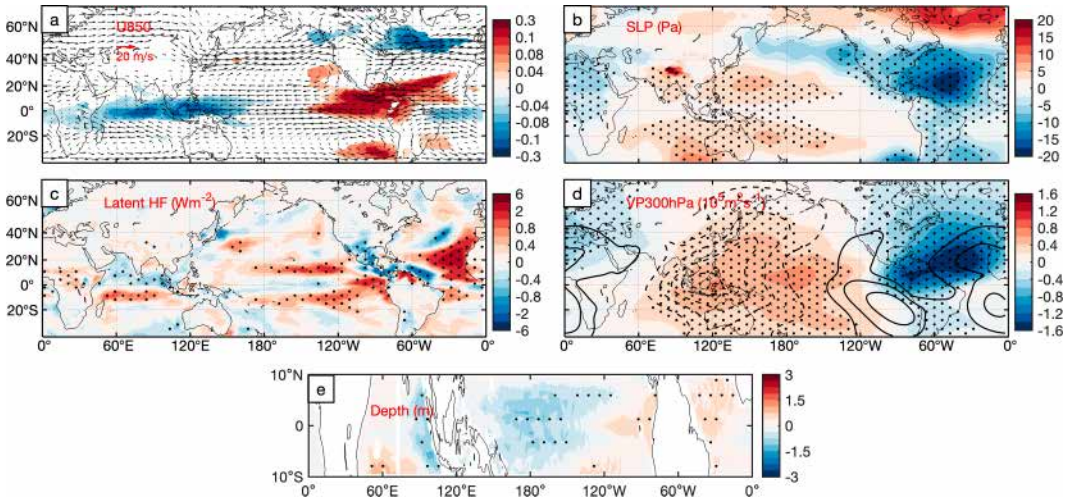

FIG. 6. Simultaneous regression in pacemaker experiments on the tropical AMV index, $\overline{T_{\text{trop}}}(t)$, of 10-yr high-pass-filtered ensemble-mean (a) zonal wind at 850 hPa (shading; m s^{-1}), (b) SLP (Pa), (c) latent heat flux, positive upward (W m^{-2}), (d) velocity potential at 300 hPa (shading; 10^5 m^2 s^{-1}), and (e) depth of the 20°C isotherm (m). In (a), only 5% significant anomalies are shown, and vectors indicate climatological surface wind at 850 hPa. In (d), solid (dashed) contours represent positive (negative) climatological velocity potential at 300 hPa, starting at $\pm 10 \times 10^5$ m^2 s^{-1} with an interval of 10×10^5 m^2 s^{-1}, and zero contour is omitted. Stipples indicate 5% significance.

tropical Atlantic Ocean (Fig. 2f) drives increased latent heat flux (Fig. 6c), consistent with the negative heat flux feedback (Frankignoul and Kestenare 2002; Park et al. 2005). The resulting diabatic heating intensifies convection and drives a large-scale atmospheric response, as captured by the regressions of the 850-hPa zonal wind and SLP onto $\overline{T_{\text{trop}}}$ (Figs. 6a,b). This response resembles the linear response to an off-equatorial heat source, as discussed by Gill (1980), with a low pressure center located slightly west of the tropical heating over the Atlantic Ocean and weakened trade winds associated with equatorial Rossby wave propagation over a region extending from the western tropical Atlantic to the eastern tropical Pacific. Meanwhile, westerlies weaken around 50°N over the North Atlantic. Anomalous equatorial easterlies linked to damped Kelvin wave propagation are also visible east of the tropical North Atlantic heat source, reaching as far as the western equatorial Pacific. These easterlies drive poleward Ekman transport on both sides of the equator, inducing equatorial upwelling, consistent with the shallower thermocline in the central Pacific (Fig. 6e). Over the Indian Ocean north of the equator, the climatological wind speed weakens (Fig. S2) and reduces local evaporation, which leads to downward heat flux (Fig. 6c) and northward Ekman transport, promoting positive SST anomalies (Figs. 2f,i). In contrast, the accelerated winds south of the equator tend to enhance evaporation (Fig. 6c), but its impact on SST might be largely balanced by southward Ekman advection. A similar mechanism connecting tropical North Atlantic heating to positive SST anomalies in the north Indian Ocean was discussed by Li et al. (2016). In addition, positive latent heat flux anomalies are simulated on both sides of the equator in the eastern tropical Pacific (Fig. 6c), promoting local cooling at the surface. However, this expected cooling is not reflected in the subsequent SST changes (Fig. 2i), likely due to the equatorward Ekman flow driven by the weakened easterly winds (Fig. 6a). Residual internal variability in the eastern tropical Pacific might also offset the effect of the heat flux anomalies.

Changes in the large-scale tropical circulation are illustrated by the velocity potential at 300 hPa (Fig. 6d). The Laplacian of the upper-troposphere velocity potential is equal to the negative of horizontal wind divergence. Therefore, a negative (positive) velocity potential anomaly indicates large-scale ascending (subsiding) air. In the pacemaker experiment, the negative velocity potential over the tropical Atlantic suggests rising motions driven by more frequent atmospheric convection, while the broad positive velocity potential anomaly above the Pacific Ocean indicates slightly weakened convection. In the western-to-central Pacific, elongated positive SLP anomalies with maximum amplitude around 30° off the equator and weak values along the equator (Fig. 6b) are consistent with reduced atmospheric convection and the ocean–atmosphere feedback linking the Indo-Pacific warm pool SST to the western Pacific subtropical high (Wang et al. 2013; Gan et al. 2022).

As illustrated for a lag of 6 months, the tropical Atlantic warming decreases with increasing lag (Fig. 7a), and correspondingly, atmospheric diabatic heating (not shown), anomalous westerlies above the eastern equatorial Pacific (Fig. 7c), and large-scale ascent (Figs. 7d,e) over the Atlantic Ocean have weakened. The early warming in the northern Indian Ocean persists, likely leading to the onset of ascending motion over India (Figs. 7d,e), and it has extended into the northwestern tropical Pacific (Fig. 7a) due to an anomalous convergence of ocean heat transport. The easterlies above the Indo-Pacific have weakened but propagated eastward to 120°W (Fig. 7c), shifting the thermocline shallowing eastward (Fig. 7b).

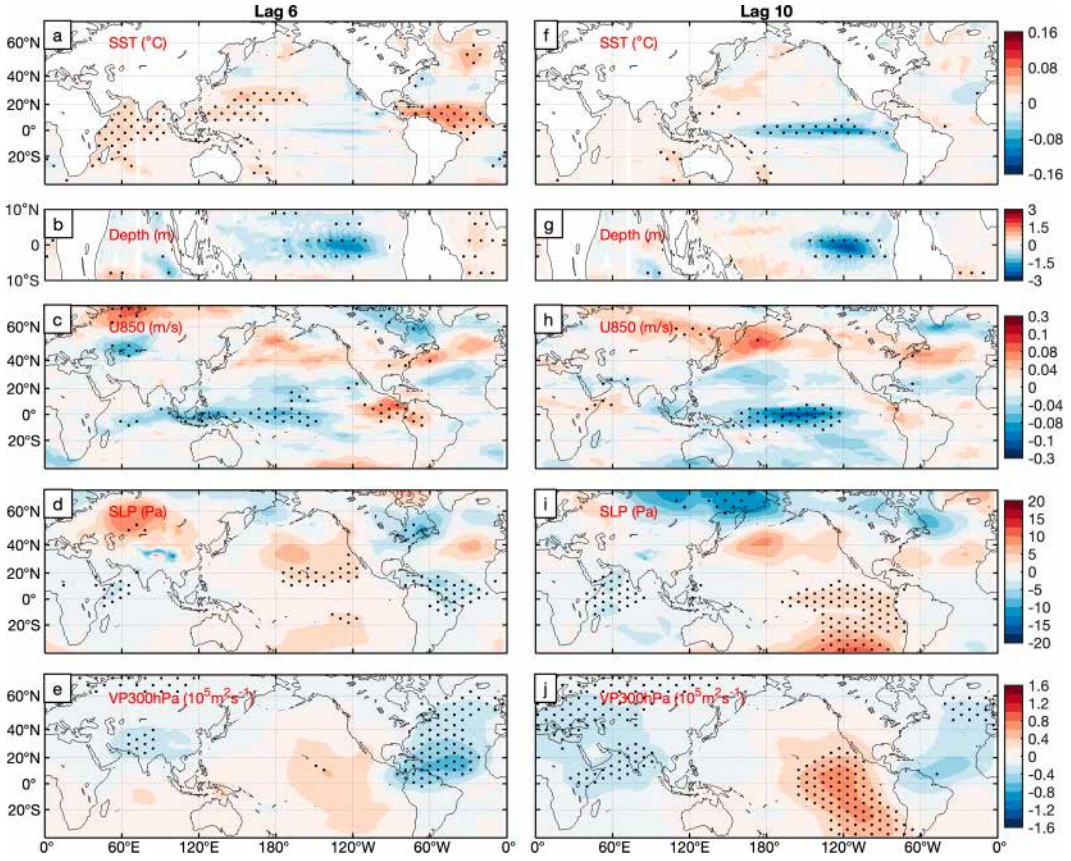

FIG. 7. As in Fig. 6, but at a lag of (a)–(e) 6 months and (f)–(j) 10 months for (first row) SST, (second row) thermocline depth, (third row) U850, (fourth row) SLP, and (fifth row) velocity potential at 300 hPa, based on 10-yr high-pass-filtered ensemble-mean pacemaker experiments.

Between lag 6 and lag 10, the North Atlantic tropical SST anomaly (Fig. 7f) and the associated large-scale atmosphere ascent (Figs. 7i,j) gradually vanish. However, the anomalous ascent over the northern Indian Ocean and midlatitude Eurasia intensifies and coincides with increased descent over the eastern Pacific (Fig. 7j). This east–west overturning pattern strengthens the Walker Circulation, promoting the anomalous easterlies in the western and central equatorial Pacific (Fig. 7h). The intensification and eastward movement of the easterlies lead to a further eastward shift of the equatorial thermocline and cooling in most of the equatorial Pacific (Fig. 7g). These changes lead to the establishment of a La Niña–like SST anomaly (Zhu et al. 2015).

The La Niña conditions continue to intensify probably via the Bjerknes feedback and reach a peak around lag 14, consistent with the cross correlation between AMV and the Niño-3 index (Fig. 3b), alongside the negative phase of the Southern Oscillation (Figs. 8a,d). The anomalous tropical Pacific easterlies have extended westward above Indonesia (Fig. 8c), while the equatorial Pacific thermocline becomes shallower in the east and deeper in the west (Fig. 8b). Positive thermocline anomalies in the west Pacific on both sides of the equator are typical of the Rossby wave response during ENSO events (Jin 1997), confirming the important role of ocean dynamics in sustaining the surface cooling in the eastern Pacific (Fig. 8a). East of the La Niña anomaly, over the equatorial South America and the equatorial Atlantic, anomalous equatorial westerlies have appeared, consistent with the circulation adjustment to ocean temperature changes proposed by Gill (1980). Also noteworthy is an anticyclonic SLP perturbation and dipolar wind anomalies off northwestern America that have some resemblance with the weakening of the Aleutian low by La Niña teleconnections, although these features are too small and located too far southeast. Nonetheless, they may contribute to the weak warming in the western and central North Pacific (Fig. 8a).

As suggested by the cross correlation between $\overline{T_{\text{trop}}}$ and Niño-3 (Fig. 3b), the La Niña SST anomaly then gradually decays. By lag 21, much of the negative SST anomalies in the eastern tropical Pacific have lost significance, although equatorial cooling remains significant in the central and western Pacific (Fig. 9a), and the weakening of the Aleutian low (Fig. 9b) has driven cold air southward advection and coastal upwelling along northwestern America, so that the SST anomaly has started resembling a negative PDO pattern, albeit with too weak warming in the Kuroshio–Oyashio extension region (Fig. 9a) compared to the typical PDO pattern (Mantua et al. 1997). Lag correlation between $\overline{T_{\text{trop}}}$ and the PDO time series

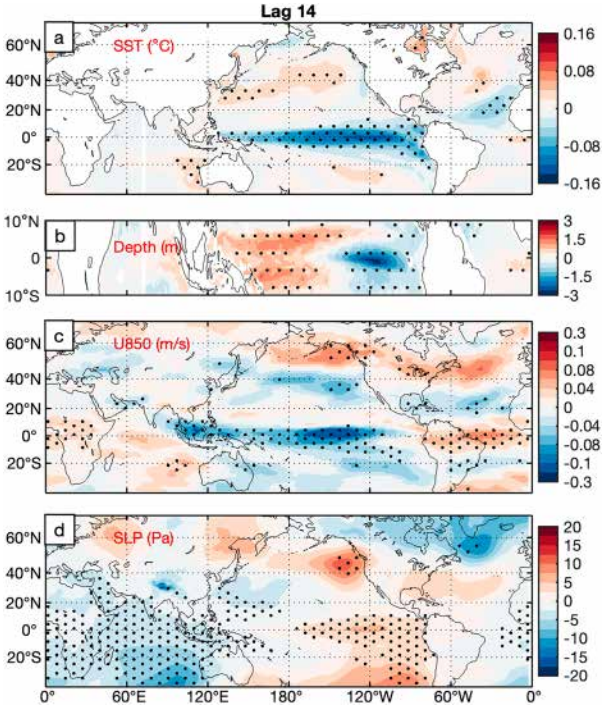

FIG. 8. As in Fig. 7, but for lag 14 for (first row) SST, (second row) thermocline depth, (third row) U850, and (fourth row) SLP, based on 10-yr high-pass-filtered ensemble-mean pacemaker experiments.

(defined as the first principal component of ensemble-mean SST anomalies in the North Pacific 20°–70°N) shows that the PDO significantly lags the tropical AMV by 21–25 months, with a peak at lag 23 (Fig. 9c, black curve). The PDO pattern is more evident at lag 23 (not shown), by which time the Aleutian low has slightly dissipated, as expected from the typical lag between atmospheric forcing and oceanic response. The PDO thus follows the fast La Niña response by about 10 months. A similar negative correlation between tropical AMV and PDO is found in (observed) nudging SST after removal of global warming, albeit without 5% significance (Fig. 9c, red curve), presumably because our use of ensemble means had strongly reduced unrelated natural PDO variability.

It should be noted that the 2-yr lag between the tropical AMV and the PDO is not inconsistent with the relationships obtained with 10-yr low-pass-filtered data (Fig. 10), albeit with slightly different patterns than in Figs. 8 and 9 as the dominant warming appears in the western extratropical Pacific and cooling off North America is negligible (Fig. 10a), while the negative correlation consistently peaks when tropical AMV leads by about 22 months (Fig. 10b). However, the persistence of the SST patterns in the low-pass-filtered analysis provides little physical insight and stresses that the chain of events could be better established through the use of high-pass-filtered data.

In addition, we applied a bootstrap-style subsampling approach (Deser et al. 2017, 2018) to validate the robustness of responses and mechanisms described above. Specifically, we generated 100 randomly selected subsets (with replacement) of eight pacemaker members drawn from the available 10-member ensemble. The key correlation and regression results remain statistically significant across these subsets (not shown), which indicates that our findings most likely represent a statistically robust chain of responses and are not artifacts of ensemble composition.

5. Conclusions and discussion

In this study, we explored the oceanic response to the observed Atlantic multidecadal variability (AMV) using transient pacemaker experiments with the IPSL-CM6A-LR climate model. In these experiments, the SSTs in the Atlantic between 10° and 65°N are nudged to the model climatology plus time-varying observed SST anomalies, using a 10-member ensemble with historical forcings from 1920 to 2014. To elucidate the mechanism of the AMV influence on remote regions, we analyzed 10-yr high-pass data and separately considered the impacts of the full AMV SST anomaly and its tropical and

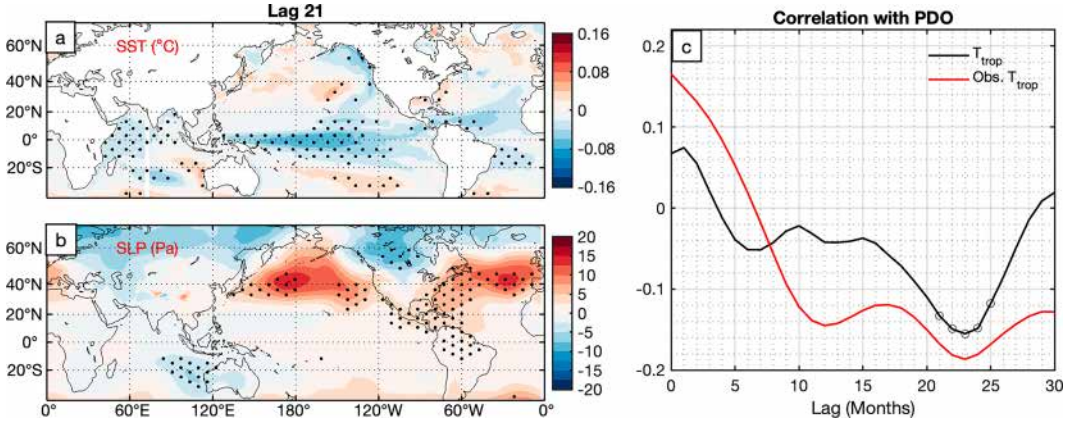

FIG. 9. Regression of (a) SST and (b) SLP on $\overline{T_{\text{trop}}}(t)$ at lag 21 in pacemaker experiments. (c) Cross correlation between $\overline{T_{trop}}(t)$ and PDO in the 10-yr high-pass-filtered pacemaker ensemble-mean SST (black) and 10-yr high-pass-filtered ERSSTv4 dataset (red) during the same period. Dots or circles indicate 5% significance.

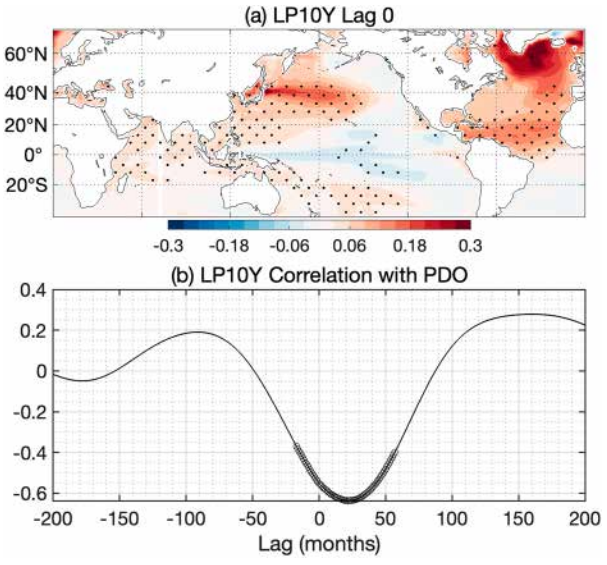

FIG. 10. (a) In phase regression of 10-yr low-pass-filtered SST (°C) onto 10-yr low-pass-filtered tropical AMV (similarly defined) in pacemaker experiments. (b) Lead–lag correlation between 10-yr low-pass-filtered PDO and 10-yr low-pass-filtered tropical AMV in the pacemaker experiment. AMV leads at positive lag. Stipples in (a) and circles in (b) indicate statistical significance at the 5% level.

extratropical parts. As the extratropical component was found to have negligible interbasin influence, we focused on the impact of the tropical AMV, as represented by the $T_{\text{trop}}(t)$ index.

Observations and a control simulation with the same climate model reveal that a positive Niño-3 index (El Niño) leads a positive T_{trop} with a maximum correlation at about 6-month lead, while the latter leads a negative Niño-3 (La Niña) peaking at about 12-month lag. Yet, the causality is difficult to establish, in particular since the lag difference of about 18 months between the positive and negative correlations broadly corresponds to the quasi-oscillatory character of the Niño-3 index. In the ensemble mean of the pacemaker experiments, SST nudging significantly reduces the positive correlation between the two tropical basins when the Pacific leads but maintains a similar negative correlation when the Pacific lags. This suggests an effective impact of the Atlantic on the Pacific. Nevertheless, persistent positive correlation around lag 0 suggests that internal variability still contributes to the tropical AMV even with an ensemble averaging over 10 members. Using a simple slab mixed layer model, we show that, although ENSO and local atmospheric forcing of the tropical AMV are not entirely removed by the ensemble averaging, they play little role, and the ensemble-mean tropical AMV is primarily forced by the nudging. Hence, AMV impacts can be reliably assessed by only considering ensemble means of 10 members, and the significant negative correlation with Niño-3 when $\overline{T_{\text{trop}}}$ leads by about 14 months can be confidently interpreted as an equatorial Pacific response to the tropical AMV.

To investigate the mechanisms linking the tropical AMV to the Indo-Pacific basin and explain the negative correlation when $\overline{T_{\text{trop}}}$ leads ENSO, we use lag regressions. We identify four distinct phases following a positive tropical AMV: phase 1 (0–6-month lag) reflects a fast response of the western Indo-Pacific Ocean; phase 2 (7–10-month lag) shows the establishment of La Niña–like SST anomalies in the eastern Pacific; phase 3 (11–20-month lag) involves the strengthening and subsequent decay of La Niña conditions; phase 4 (21–25-month lag) corresponds to the establishment of a negative phase of the PDO. We describe below these phases in further detail:

Phase 1: A warm tropical AMV intensifies deep convection and leads to rising motions over the tropical Atlantic and compensatory subsidence above the western Pacific, indicating a modification of the Pacific Walker circulation. The associated wind changes broadly mimic the predictions of the classical Gill model (Gill 1980), with easterly wind anomalies in the Indo-western Pacific. The anomalous easterlies over the ocean induce poleward Ekman transport and equatorial upwelling, contributing to a shallowing of the thermocline in the Indo-western Pacific. Meanwhile, reduced wind speed over the northern Indian Ocean reduces local evaporation and causes SST warming. By a lag of 6 months, the tropical North Atlantic SST decreases, accompanied by a weakening of the associated large-scale ascent over the tropical Atlantic and an eastward propagation of the anomalous easterlies. The northern Indian Ocean warming weakens, but the warming extends eastward into the western Indo-Pacific warm pool, while the shallowing of the Pacific equatorial thermocline also progresses eastward.

Phase 2: About 7 months after the tropical AMV peak, the early warming over the north Indian Ocean extends eastward, contributing to localized ascending motion and associated strengthening of Walker circulation over the equatorial Pacific Ocean. The easterly anomalies continue to intensify, sustaining the equatorial upwelling and the shallower thermocline depth. The eastward shift of the easterly wind anomaly shifts the thermocline shallowing eastward, which reaches the eastern Pacific 9–10 months after the AMV. The resulting cooling in the eastern central Pacific marks the onset of a La Niña–like SST anomaly.

Phase 3: The cold equatorial Pacific SST anomalies build up and reach their peak at a lag of 14 months via the Bjerknes feedback. Then, the enhanced trade winds pile up warm water in the western Pacific and increase the thermocline depth, initiating the decay of La Niña, which nonetheless persists until about lag 20. Meanwhile, La Niña teleconnections drive positive SLP anomalies off northwestern America and weaken the Aleutian low.

Phase 4: The weakened Aleutian low and associated dipolar wind anomalies over the extratropical North Pacific lead to weak warming in the western and central North Pacific and also weak cooling in the Gulf of Alaska and along northwestern America. This results in SST anomalies resembling a negative PDO pattern that lags the tropical AMV by about 21 months. This PDO-like pattern remains significant until lag 25.

Several previous modeling and observational studies have pointed out that La Niña–like SST anomalies in the tropical Pacific can be induced by warm AMV conditions (Kucharski et al. 2016; Chafik et al. 2016; Meehl et al. 2021; Ruprich-Robert et al. 2021) or warm equatorial Atlantic (Rodríguez-Fonseca et al. 2009; Martín-Rey et al. 2014; Li et al. 2016). The mechanisms identified in the first two phases of our study align with Li et al. (2016), where La Niña was triggered by surface wind anomalies in the Indian Ocean forced by tropical Atlantic diabatic heating and later strengthened by the Bjerknes feedback. While most previous studies have emphasized a direct pathway from the tropical Atlantic to the tropical Pacific via the reorganizations of the Walker circulation, both Li et al. (2016) and our work highlight an important intermediary role of the Indian Ocean. The persistence of the Indian Ocean warming sustains atmospheric ascent in that region when Atlantic anomalies are dissipating, thereby reinforcing the zonal pressure gradient and anchoring the anomalous Walker circulation. Without this intermediate step, we suspect that the Atlantic influence on the Pacific would likely be weaker or more transient. Zhang and Delworth (2007) proposed an extratropical pathway for the impact of the AMV on the North Pacific mostly through higher North Pacific SLP and warmer Kuroshio–Oyashio extension, but we found no evidence of extratropical AMV influence, consistent with several findings that the AMV rather impacts the North Pacific through a tropical pathway via trade wind anomalies (e.g., Yang et al. 2020; An et al. 2021).

The transition to a negative PDO response suggested in phase 4 may seem consistent with the impact of AMV on the PDO documented in several observational studies (d'Orgeville and Peltier 2007; Wu et al. 2011; Marini and Frankignoul 2014), but unlike in the present study, the statistical significance was limited, perhaps in part because our use of ensemble means had strongly reduced unrelated natural PDO variability. Indeed, based on data assimilation experiments in climate models, Johnson et al. (2020) estimated that only about one-third of the PDO variance originates from the Atlantic Ocean. More importantly, most of the above studies found that the response to the AMV was much slower than the 2–3 years found in our pacemaker experiments, needing 12–14 years to establish. We found no significant relationship when AMV leads by 12–14 years. This is consistent with recent studies that suggested that this long time-scale relationship, if really significant, results from inadequate removal of the signals due to anthropogenic and other external forcing (Frankignoul et al. 2017; Fenske and Clement 2022; Deser and Phillips 2023), as discussed in section 1. Although the global warming signal was removed in our study based on historical simulations that had a slightly different behavior than the pacemaker simulations (Fig. S1), it should affect little the AMV–PDO connections found here at a much shorter time scale.

It is worth noting that the tropical AMV warming decays during phase 2 and turns into a cooling phase during phases 3 and 4 in our analysis. The peak of La Niña conditions and the subsequent development of the PDO pattern thus occur after the Atlantic forcing has subsided. This timing underscores a key feature of the transient pacemaker experiments, which allow the AMV to evolve and decay. In contrast, idealized pacemaker experiments impose fixed AMV conditions throughout, making it difficult to assess the role of delayed or memory-driven responses.

While increasing the ensemble size would further enhance statistical robustness, particularly for detecting transient or spatially localized atmospheric signals, the computational cost of running large ensembles can be prohibitive, especially for higher resolution or computationally demanding models. Our multifaceted validation strategy, including statistical modeling and bootstrap-style subsampling, demonstrates that a 10-member ensemble is sufficient to isolate the forced AMV response, in this context. We argue that this approach provides a practical and scalable framework for broader applications. In addition to ensemble size, multimodel comparisons of idealized pacemaker experiments have revealed significant intermodel differences in simulated tropical responses (Ruprich-Robert et al. 2021; Hodson et al. 2022). These variations likely arise from differences in the amount of moist static energy injection from the tropical Atlantic surface to the upper troposphere, shaped by the rainfall climatologies specific to each model (Ruprich-Robert et al. 2021). These discrepancies highlight the need to use a range of models and experimental frameworks to evaluate the robustness of the AMV–Pacific link. We advocate here for more modeling groups running such pacemaker experiments in a coordinated way.

While our study used the linear regression analysis, future work should also explore potential nonlinearities in the interbasin connections. Previous studies have often relied on comparisons between AMV+ and AMV− phases or neutral states, which may also overlook potential nonlinear interactions between AMV, ENSO, and PDO. For instance, some research has suggested that the modulation of the ENSO by the AMV may exhibit nonlinear characteristics (Geng et al. 2020). This raises the possibility that the strength or even the sign of Pacific–AMV teleconnections could vary depending on the specific AMV state, rather than following a simple linear relationship. To better understand these evolving connections, future studies could explore alternative methods beyond linear regression.

Last, examining the temporal stability and potential decadal modulation of the AMV–Pacific connection could provide new insights into the mechanisms and predictability of this important teleconnection pattern. From a practical point, note that a recently developed dataset (DCENT) spanning since 1850 reveals that the apparent drops in SST and global-mean temperature during 1940–50, commonly seen in many historical datasets, are likely spurious artifacts caused by data inhomogeneities (Chan et al. 2024). Future work could benefit from cross validation with DCENT to reassess and potentially correct for such early period anomalies in AMV reconstructions.

Acknowledgments. Support to W. Jiang from National Key R&D Program of China (Grant 2023YFF0805102) is

gratefully acknowledged. Most of this work was done, while W. Jiang was a postdoctoral fellow at LOCEAN and supported by the JPI climate/JPI ocean ROADMAP project (Grant ANR-19-JPOC-003). This work was granted access to the HPC resources of TGCC under the allocation 2024-A0150107403 made by GENCI.

Data availability statement. Pacemaker experiment data are available through ESGF, from the dcppC-atl-pacemaker experiments in DCPP-C panel of CMIP6 (https://esgf-node.llnl.gov/projects/cmip6/). All codes used for data analysis and figures are available online (https://github.com/WeiminJiang/pacemaker).

REFERENCES

An, X., B. Wu, T. Zhou, and B. Liu, 2021: Atlantic multidecadal oscillation drives interdecadal Pacific variability via tropical atmospheric bridge. *J. Climate*, **34**, 5543–5553, https://doi.org/10.1175/JCLI-D-20-0983.1.

Bellomo, K., L. N. Murphy, M. A. Cane, A. C. Clement, and L. M. Polvani, 2018: Historical forcings as main drivers of the Atlantic multidecadal variability in the CESM large ensemble. *Climate Dyn.*, **50**, 3687–3698, https://doi.org/10.1007/s00382-017-3834-3.

Bellucci, A., A. Mariotti, and S. Gualdi, 2017: The role of forcings in the twentieth-century North Atlantic multidecadal variability: The 1940–75 North Atlantic cooling case study. *J. Climate*, **30**, 7317–7337, https://doi.org/10.1175/JCLI-D-16-0301.1.

Boer, G. J., and Coauthors, 2016: The Decadal Climate Prediction Project (DCPP) contribution to CMIP6. *Geosci. Model Dev.*, **9**, 3751–3777, https://doi.org/10.5194/gmd-9-3751-2016.

Bonnet, R., O. Boucher, J. Deshayes, G. Gastineau, F. Hourdin, J. Mignot, J. Servonnat, and D. Swingedouw, 2021: Presentation and evaluation of the IPSL-CM6A-LR ensemble of extended historical simulations. *J. Adv. Model. Earth Syst.*, **13**, e2021MS002565, https://doi.org/10.1029/2021MS002565.

——, O. C. M. McKenna, and A. C. Maycock, 2024: Model spread in multidecadal North Atlantic oscillation variability connected to stratosphere–troposphere coupling. *Wea. Climate Dyn.*, **5**, 913–926, https://doi.org/10.5194/wcd-5-913-2024.

Booth, B. B. B., N. J. Dunstone, P. R. Halloran, T. Andrews, and N. Bellouin, 2012: Aerosols implicated as a prime driver of twentieth-century North Atlantic climate variability. *Nature*, **484**, 228–232, https://doi.org/10.1038/nature10946.

Boucher, O., and Coauthors, 2020: Presentation and evaluation of the IPSL-CM6A-LR climate model. *J. Adv. Model. Earth Syst.*, **12**, e2019MS002010, https://doi.org/10.1029/2019MS002010.

Buckley, M. W., and J. Marshall, 2016: Observations, inferences, and mechanisms of the Atlantic meridional overturning circulation: A review. *Rev. Geophys.*, **54**, 5–63, https://doi.org/10.1002/2015RG000493.

Chafik, L., S. Häkkinen, M. H. England, J. A. Carton, S. Nigam, A. Ruiz-Barradas, A. Hannachi, and L. Miller, 2016: Global linkages originating from decadal oceanic variability in the subpolar North Atlantic. *Geophys. Res. Lett.*, **43**, 10 909–10 919, https://doi.org/10.1002/2016GL071134.

Chan, D., G. Gebbie, P. Huybers, and E. C. Kent, 2024: A dynamically consistent Ensemble of temperature at the earth surface since 1850 from the DCENT dataset. *Sci. Data*, **11**, 953, https://doi.org/10.1038/s41597-024-03742-x.

Clement, A., K. Bellomo, L. N. Murphy, M. A. Cane, T. Mauritsen, G. Rädel, and B. Stevens, 2015: The Atlantic multidecadal oscillation without a role for ocean circulation. *Science*, **350**, 320–324, https://doi.org/10.1126/science.aab3980.

Coburn, J., and S. C. Pryor, 2021: Differential credibility of climate modes in CMIP6. *J. Climate*, **34**, 8145–8164, https://doi.org/10.1175/JCLI-D-21-0359.1.

de Boyer Montégut, C., G. Madec, A. S. Fischer, A. Lazar, and D. Iudicone, 2004: Mixed layer depth over the global ocean: An examination of profile data and a profile-based climatology. *J. Geophys. Res.*, **109**, C12003, https://doi.org/10.1029/2004JC002378.

Deser, C., and A. S. Phillips, 2023: Spurious Indo-Pacific connections to internal Atlantic multidecadal variability introduced by the global temperature residual method. *Geophys. Res. Lett.*, **50**, e2022GL100574, https://doi.org/10.1029/2022GL100574.

——, I. R. Simpson, K. A. McKinnon, and A. S. Phillips, 2017: The Northern Hemisphere extratropical atmospheric circulation response to ENSO: How well do we know it and how do we evaluate models accordingly? *J. Climate*, **30**, 5059–5082, https://doi.org/10.1175/JCLI-D-16-0844.1.

——, ——, A. S. Phillips, and K. A. McKinnon, 2018: How well do we know ENSO's climate impacts over North America, and how do we evaluate models accordingly? *J. Climate*, **31**, 4991–5014, https://doi.org/10.1175/JCLI-D-17-0783.1.

d'Orgeville, M., and W. R. Peltier, 2007: On the Pacific decadal oscillation and the Atlantic multidecadal oscillation: Might they be related? *Geophys. Res. Lett.*, **34**, L23705, https://doi.org/10.1029/2007GL031584.

Dunstone, N. J., D. M. Smith, and R. Eade, 2011: Multi-year predictability of the tropical Atlantic atmosphere driven by the high latitude North Atlantic Ocean. *Geophys. Res. Lett.*, **38**, L14701, https://doi.org/10.1029/2011GL047949.

England, M. H., and Coauthors, 2014: Recent intensification of wind-driven circulation in the Pacific and the ongoing warming hiatus. *Nat. Climate Change*, **4**, 222–227, https://doi.org/10.1038/nclimate2106.

Fenske, T., and A. Clement, 2022: No internal connections detected between low frequency climate modes in North Atlantic and North Pacific basins. *Geophys. Res. Lett.*, **49**, e2022GL097957, https://doi.org/10.1029/2022GL097957.

Frankignoul, C., and K. Hasselmann, 1977: Stochastic climate models, Part II Application to sea-surface temperature anomalies and thermocline variability. *Tellus*, **29**, 289–305, https://doi.org/10.3402/tellusa.v29i4.11362.

——, and E. Kestenare, 2002: The surface heat flux feedback. Part I: Estimates from observations in the Atlantic and the North Pacific. *Climate Dyn.*, **19**, 633–647, https://doi.org/10.1007/s00382-002-0252-x.

——, G. Gastineau, and Y.-O. Kwon, 2017: Estimation of the SST response to anthropogenic and external forcing and its impact on the Atlantic multidecadal oscillation and the Pacific decadal oscillation. *J. Climate*, **30**, 9871–9895, https://doi.org/10.1175/JCLI-D-17-0009.1.

Gan, Q., L. Wang, J. C.-H. Leung, J. Weng, and B. Zhang, 2022: Recent weakening relationship between the springtime Indo-Pacific warm pool SST zonal gradient and the subsequent summertime western Pacific subtropical high. *Int. J. Climatol.*, **42**, 10 173–10 194, https://doi.org/10.1002/joc.7890.

Gastineau, G., and C. Frankignoul, 2015: Influence of the North Atlantic SST variability on the atmospheric circulation during the twentieth century. *J. Climate*, **28**, 1396–1416, https://doi.org/10.1175/JCLI-D-14-00424.1.

——, F. D'Andrea, and C. Frankignoul, 2013: Atmospheric response to the North Atlantic Ocean variability on seasonal to decadal time scales. *Climate Dyn.*, **40**, 2311–2330, https://doi.org/10.1007/s00382-012-1333-0.

Geng, X., W. Zhang, F.-F. Jin, M. F. Stuecker, and A. F. Z. Levine, 2020: Modulation of the relationship between ENSO and its combination mode by the Atlantic multidecadal oscillation. *J. Climate*, **33**, 4679–4695, https://doi.org/10.1175/JCLI-D-19-0740.1.

Gill, A. E., 1980: Some simple solutions for heat-induced tropical circulation. *Quart. J. Roy. Meteor. Soc.*, **106**, 447–462, https://doi.org/10.1002/qj.49710644905.

Häkkinen, S., P. B. Rhines, and D. L. Worthen, 2011: Atmospheric blocking and Atlantic multidecadal ocean variability. *Science*, **334**, 655–659, https://doi.org/10.1126/science.1205683.

Hodson, D. L. R., and Coauthors, 2022: Coupled climate response to Atlantic multidecadal variability in a multi-model multi-resolution ensemble. *Climate Dyn.*, **59**, 805–836, https://doi.org/10.1007/s00382-022-06157-9.

Huang, B., and Coauthors, 2016: Further exploring and quantifying uncertainties for Extended Reconstructed Sea Surface Temperature (ERSST) version 4 (v4). *J. Climate*, **29**, 3119–3142, https://doi.org/10.1175/JCLI-D-15-0430.1.

Jin, F.-F., 1997: An equatorial ocean recharge paradigm for ENSO. Part I: Conceptual model. *J. Atmos. Sci.*, **54**, 811–829, https://doi.org/10.1175/1520-0469(1997)054<0811:AEORPF>2.0.CO;2.

Johnson, Z. F., Y. Chikamoto, S.-Y. S. Wang, M. J. McPhaden, and T. Mochizuki, 2020: Pacific decadal oscillation remotely forced by the equatorial Pacific and the Atlantic Oceans. *Climate Dyn.*, **55**, 789–811, https://doi.org/10.1007/s00382-020-05295-2.

Kim, W. M., S. Yeager, and G. Danabasoglu, 2020: Atlantic multidecadal variability and associated climate impacts initiated by ocean thermohaline dynamics. *J. Climate*, **33**, 1317–1334, https://doi.org/10.1175/JCLI-D-19-0530.1.

Klavans, J. M., A. C. Clement, M. A. Cane, and L. N. Murphy, 2022: The evolving role of external forcing in North Atlantic SST variability over the last millennium. *J. Climate*, **35**, 2741–2754, https://doi.org/10.1175/JCLI-D-21-0338.1.

Kosaka, Y., and S.-P. Xie, 2013: Recent global-warming hiatus tied to equatorial Pacific surface cooling. *Nature*, **501**, 403–407, https://doi.org/10.1038/nature12534.

Kucharski, F., and Coauthors, 2016: Atlantic forcing of Pacific decadal variability. *Climate Dyn.*, **46**, 2337–2351, https://doi.org/10.1007/s00382-015-2705-z.

Kushnir, Y., R. Seager, M. Ting, N. Naik, and J. Nakamura, 2010: Mechanisms of tropical Atlantic SST influence on North American precipitation variability. *J. Climate*, **23**, 5610–5628, https://doi.org/10.1175/2010JCLI3172.1.

Kwon, Y.-O., H. Seo, C. C. Ummenhofer, and T. M. Joyce, 2020: Impact of multidecadal variability in Atlantic SST on winter atmospheric blocking. *J. Climate*, **33**, 867–892, https://doi.org/10.1175/JCLI-D-19-0324.1.

Levine, A. F. Z., M. J. McPhaden, and D. M. W. Frierson, 2017: The impact of the AMO on multidecadal ENSO variability. *Geophys. Res. Lett.*, **44**, 3877–3886, https://doi.org/10.1002/2017GL072524.

Li, X., S.-P. Xie, S. T. Gille, and C. Yoo, 2016: Atlantic-induced pan-tropical climate change over the past three decades. *Nat. Climate Change*, **6**, 275–279, https://doi.org/10.1038/nclimate2840.

Liu, G., Y.-O. Kwon, C. Frankignoul, and J. Lu, 2023: Understanding the drivers of Atlantic multidecadal variability using a stochastic model hierarchy. *J. Climate*, **36**, 1043–1058, https://doi.org/10.1175/JCLI-D-22-0309.1.

Mantua, N. J., S. R. Hare, Y. Zhang, J. M. Wallace, and R. C. Francis, 1997: A Pacific interdecadal climate oscillation with impacts on salmon production. *Bull. Amer. Meteor. Soc.*, **78**, 1069–1079, https://doi.org/10.1175/1520-0477(1997)078<1069:APICOW>2.0.CO;2.

Marini, C., and C. Frankignoul, 2014: An attempt to deconstruct the Atlantic multidecadal oscillation. *Climate Dyn.*, **43**, 607–625, https://doi.org/10.1007/s00382-013-1852-3.

Martín-Rey, M., B. Rodríguez-Fonseca, I. Polo, and F. Kucharski, 2014: On the Atlantic–Pacific Niños connection: A multidecadal modulated mode. *Climate Dyn.*, **43**, 3163–3178, https://doi.org/10.1007/s00382-014-2305-3.

McGregor, S., M. F. Stuecker, J. B. Kajtar, M. H. England, and M. Collins, 2018: Model tropical Atlantic biases underpin diminished Pacific decadal variability. *Nat. Climate Change*, **8**, 493–498, https://doi.org/10.1038/s41558-018-0163-4.

Meehl, G. A., and Coauthors, 2021: Atlantic and Pacific tropics connected by mutually interactive decadal-timescale processes. *Nat. Geosci.*, **14**, 36–42, https://doi.org/10.1038/s41561-020-00669-x.

Menary, M. B., and A. A. Scaife, 2014: Naturally forced multidecadal variability of the Atlantic meridional overturning circulation. *Climate Dyn.*, **42**, 1347–1362, https://doi.org/10.1007/s00382-013-2028-x.

Murphy, L. N., J. M. Klavans, A. C. Clement, and M. A. Cane, 2021: Investigating the roles of external forcing and ocean circulation on the Atlantic multidecadal SST variability in a large ensemble climate model hierarchy. *J. Climate*, **34**, 4835–4849, https://doi.org/10.1175/JCLI-D-20-0167.1.

O'Reilly, C. H., M. Patterson, J. Robson, P. A. Monerie, D. Hodson, and Y. Ruprich-Robert, 2023: Challenges with interpreting the impact of Atlantic multidecadal variability using SST-restoring experiments. *npj Climate Atmos. Sci.*, **6**, 14, https://doi.org/10.1038/s41612-023-00335-0.

Otterå, O. H., M. Bentsen, H. Drange, and L. Suo, 2010: External forcing as a metronome for Atlantic multidecadal variability. *Nat. Geosci.*, **3**, 688–694, https://doi.org/10.1038/ngeo955.

Park, S., C. Deser, and M. A. Alexander, 2005: Estimation of the surface heat flux response to sea surface temperature anomalies over the global oceans. *J. Climate*, **18**, 4582–4599, https://doi.org/10.1175/JCLI3521.1.

Peings, Y., and G. Magnusdottir, 2014: Forcing of the wintertime atmospheric circulation by the multidecadal fluctuations of the North Atlantic Ocean. *Environ. Res. Lett.*, **9**, 034018, https://doi.org/10.1088/1748-9326/9/3/034018.

Pyper, B. J., and R. M. Peterman, 1998: Comparison of methods to account for autocorrelation in correlation analyses of fish data. *Can. J. Fish. Aquat. Sci.*, **55**, 2127–2140, https://doi.org/10.1139/f98-104.

Robson, J., R. Sutton, M. B. Menary, and M. W. K. Lai, 2023: Contrasting internally and externally generated Atlantic multidecadal variability and the role for AMOC in CMIP6 historical simulations. *Philos. Trans. Roy. Soc.*, **A381**, 20220194, https://doi.org/10.1098/rsta.2022.0194.

Rodríguez-Fonseca, B., I. Polo, J. García-Serrano, T. Losada, E. Mohino, C. R. Mechoso, and F. Kucharski, 2009: Are Atlantic Niños enhancing Pacific ENSO events in recent decades? *Geophys. Res. Lett.*, **36**, L20705, https://doi.org/10.1029/2009GL040048.

Ruprich-Robert, Y., R. Msadek, F. Castruccio, S. Yeager, T. Delworth, and G. Danabasoglu, 2017: Assessing the climate impacts of the observed Atlantic multidecadal variability using the GFDL CM2.1 and NCAR CESM1 global coupled models. *J. Climate*, **30**, 2785–2810, https://doi.org/10.1175/JCLI-D-16-0127.1.

——, and Coauthors, 2021: Impacts of Atlantic multidecadal variability on the tropical Pacific: A multi-model study. *npj Climate Atmos. Sci.*, **4**, 33, https://doi.org/10.1038/s41612-021-00188-5.

Schubert, S., and Coauthors, 2009: A U.S. CLIVAR Project to assess and compare the responses of global climate models to drought-related SST forcing patterns: Overview and results. *J. Climate*, **22**, 5251–5272, https://doi.org/10.1175/2009JCLI3060.1.

Si, D., A. Hu, D. Jiang, and X. Lang, 2023: Atmospheric teleconnection associated with the Atlantic multidecadal variability in summer: Assessment of the CESM1 model. *Climate Dyn.*, **60**, 1043–1060, https://doi.org/10.1007/s00382-022-06331-z.

Sutton, R. T., and B. Dong, 2012: Atlantic Ocean influence on a shift in European climate in the 1990s. *Nat. Geosci.*, **5**, 788–792, https://doi.org/10.1038/ngeo1595.

Swingedouw, D., P. Ortega, J. Mignot, E. Guilyardi, V. Masson-Delmotte, P. G. Butler, M. Khodri, and R. Séférian, 2015: Bidecadal North Atlantic Ocean circulation variability controlled by timing of volcanic eruptions. *Nat. Commun.*, **6**, 6545, https://doi.org/10.1038/ncomms7545.

Wang, B., B. Xiang, and J.-Y. Lee, 2013: Subtropical high predictability establishes a promising way for monsoon and tropical storm predictions. *Proc. Natl. Acad. Sci. USA*, **110**, 2718–2722, https://doi.org/10.1073/pnas.1214626110.

Watanabe, M., and H. Tatebe, 2019: Reconciling roles of sulphate aerosol forcing and internal variability in Atlantic multidecadal climate changes. *Climate Dyn.*, **53**, 4651–4665, https://doi.org/10.1007/s00382-019-04811-3.

Wills, R. C. J., D. S. Battisti, K. C. Armour, T. Schneider, and C. Deser, 2020: Pattern recognition methods to separate forced responses from internal variability in climate model ensembles and observations. *J. Climate*, **33**, 8693–8719, https://doi.org/10.1175/JCLI-D-19-0855.1.

Wu, S., Z. Liu, R. Zhang, and T. L. Delworth, 2011: On the observed relationship between the Pacific decadal oscillation and the Atlantic multi-decadal oscillation. *J. Oceanogr.*, **67**, 27–35, https://doi.org/10.1007/s10872-011-0003-x.

Yang, Y.-M., S.-I. An, B. Wang, and J. H. Park, 2020: A global-scale multidecadal variability driven by Atlantic multidecadal oscillation. *Natl. Sci. Rev.*, **7**, 1190–1197, https://doi.org/10.1093/nsr/nwz216.

Zhang, R., and T. L. Delworth, 2006: Impact of Atlantic multidecadal oscillations on India/Sahel rainfall and Atlantic hurricanes. *Geophys. Res. Lett.*, **33**, L17712, https://doi.org/10.1029/2006GL026267.

——, and ——, 2007: Impact of the Atlantic multidecadal oscillation on North Pacific climate variability. *Geophys. Res. Lett.*, **34**, L23708, https://doi.org/10.1029/2007GL031601.

——, R. Sutton, G. Danabasoglu, Y. Kwon, R. Marsh, S. G. Yeager, D. E. Amrhein, and C. M. Little, 2019: A review of the role of the Atlantic meridional overturning circulation in Atlantic multidecadal variability and associated climate impacts. *Rev. Geophys.*, **57**, 316–375, https://doi.org/10.1029/2019RG000644.

Zhu, J., A. Kumar, and B. Huang, 2015: The relationship between thermocline depth and SST anomalies in the eastern equatorial Pacific: Seasonality and decadal variations. *Geophys. Res. Lett.*, **42**, 4507–4515, https://doi.org/10.1002/2015GL064220.